Sulfur Isotopic Composition of Cenozoic Seawater Sulfate

Adina Paytan,* Miriam Kastner, Douglas Campbell, Mark H. Thiemens

A continuous seawater sulfate sulfur isotope curve for the Cenozoic with a resolution of ~1 million years was generated using marine barite. The sulfur isotopic composition decreased from 19 to 17 per mil between 65 and 55 million years ago, increased abruptly from 17 to 22 per mil between 55 and 45 million years ago, remained nearly constant from 35 to ~2 million years ago, and has decreased by 0.8 per mil during the past 2 million years. A comparison between seawater sulfate and marine carbonate carbon isotope records reveals no clear systematic coupling between the sulfur and carbon cycles over one to several millions of years, indicating that changes in the burial rate of pyrite sulfur and organic carbon did not singularly control the atmospheric oxygen content over short time intervals in the Cenozoic. This finding has implications for the modeling of controls on atmospheric oxygen concentration.

Global changes in climate and atmospheric chemistry are intimately related to the sedimentary S cycle (*1, 2*). Seawater sulfate represents one of the main reservoirs of dissolved S (*3*). Evidence for large-scale transfers of S between different sedimentary reservoirs is provided by the evaporite-based isotope record of oceanic sulfate (*4–6*). Here, we present a high-resolution, continuous seawater S isotope age curve (Fig. 1) that could help to elucidate the factors affecting the cycles of S and C and atmospheric oxygen content over geologic time.

The concentration of dissolved sulfate in the ocean and its $\delta^{34}S$ value are controlled by (i) a balance between the flux of S to the oceans from continental weathering and its isotopic value [$\delta^{34}S$ of this source is variable but is typically lower than seawater, 0 to 10 per mil (*1*)], and (ii) the deposition rate of S-bearing sediments, including evaporite sulfates with $\delta^{34}S$ values approximately equal to that of seawater, and pyrite sulfide with a large isotopic fractionation signature [for example, modern $\delta^{34}S$ values of pyrites average about –20 per mil (*7*)]. Volcanism and hydrothermal activity are also sources of reduced sulfur to the ocean [$\delta^{34}S$ values of these sources vary from about 0 to 3.5 per mil (*1, 8, 9*)]. Therefore, considerable S isotopic variations can be generated. For example, during periods of enhanced pyrite formation and burial, the light S isotope is preferentially removed from the ocean and the $\delta^{34}S$ value of seawater sulfate increases. These and other fluctuations are recorded in contemporaneous evaporites and marine barite.

Suitability of barite for recording seawater sulfate isotopic composition. Records of the S isotopic composition of seawater sulfate have been obtained mostly from isotope data on marine evaporite sulfates [for reviews see (*5, 6, 10*)], but the geological record of marine evaporites is episodic, with gaps of millions of years (*5*). Evaporites are also susceptible to diagenesis, their age control is often problematic (*3*), and a purely marine origin of some is questionable (*11*). In another attempt, Burdett *et al*. (*12*) used the S isotope composition of carbonate-associated sulfate in tests of planktonic foraminifers. However, the nature of SO_4^{2-} incorporation in carbonates is not well understood (*13*), and its behavior during carbonate diagenesis is unknown. Because carbonates are susceptible to diagenetic alteration (*14*), and because biological vital effects during the incorporation of sulfate cannot be ruled out, the use of marine carbonates for establishing a record of S isotopes of seawater sulfate is also problematic.

We used marine barite, a readily available ubiquitous minor phase in deep-sea sediments (*15, 16*), for the construction of the seawater sulfate S isotope record. It continuously forms in the water column; the associated sediment ages can be determined using bio- and magnetostratigraphy; barite is not particularly susceptible to diagenetic alteration in oxic sediments (*16, 17*); S is one of its major constituents; and at Earth-surface temperatures, the fractionation factor of S between seawater and barite is small (<0.4 per mil). Furthermore, barite has been shown to reliably record the seawater Sr isotopic composition (*16*). For these reasons, marine barite is a suitable mineral for recording the history of seawater S geochemistry.

We separated marine barite from more than 20 Holocene core-top sediments from the Atlantic, Pacific, and Indian oceans, as well as from six Deep Sea Drilling Project (DSDP) cores spanning the last 65 million years (My) of Earth's history (see Fig. 1 for sample locations). Separation and purification of barite were carried out using a sequential leaching method modified from (*16*) to ensure that no sulfide S reprecipitated as barite during the procedure (*18*). The barite S was converted to silver sulfide and fluorinated to SF_6 (*19, 20*).

The mean $\delta^{34}S$ value for all core-top samples of barite was 21.18 per mil relative to the Canyon Diablo Troilite standard (Fig. 1). The $\delta^{33}S$ value is 10.82 per mil, and $\delta^{36}S$ is 39.45 per mil. The precision was ±0.20 per mil. This $\delta^{34}S$ value compares well with the modern seawater $\delta^{34}S$ value of 20.99 ± 0.25 per mil determined by (*21*). This comparison indicates that marine barite records the contemporaneous S isotopic composition of seawater. Moreover, data from older marine barite samples from different cores agree with each other at any given time (Fig. 1), suggesting that barite in these samples reliably records and preserves the S isotopic composition of seawater. Over the 65-My time interval, the crystal habit of the barite does not change, and the Sr isotopic ratios of the barites (*16*) are within the range of the published Sr isotopic record for carbonates of corresponding age. Both observations indicate that the marine barites used in our study have not significantly recrystallized over the past 65 My.

Systematics of the S isotope composition of seawater sulfate. The major features of the original evaporite-based seawater sulfate S isotope curve for the Cenozoic are seen in the new marine barite data (Fig. 1). However, the new data set, obtained at a time resolution of ~1 My, shows considerably more detail, filling significant gaps and revealing newly recognized features. The oceanic residence time of dissolved sulfate is ~20 My (*22*). Our data set indicates that substantialvariations in $\delta^{34}S$ have taken place on shorter time scales, implying that the oceans have not been at isotopic steady state with respect to sulfur. This result should be taken into account in future efforts to model the linkage between the S and C cycles and atmospheric O_2 (*1*).

The low values of $\delta^{34}S$ between 65 and 55 million years ago (Ma) indicate that during this time interval, either pyrite deposition rates were lower or there was increased input of isotopically light S to the oceans. The minimum at ~55 Ma, the Paleocene-Eocene boundary, coincides with

A. Paytan, M. Kastner, and D. Campbell are in the Geosciences Research Division, Scripps Institution of Oceanography, 9500 Gilman Drive, La Jolla, CA 92093, USA. M. H. Thiemens is in the Chemistry Department, University of California, San Diego, 9500 Gilman Drive, La Jolla, CA 92093, USA.

*To whom correspondence should be addressed. E-mail: apaytan@ucsd.edu

an important benthic foraminiferal global extinction; large, negative, short-term C isotopic excursion (Fig. 2A); a maximum in deep ocean temperature (~18°C); and intense volcanism (*23*). The largest shift in the S isotope ratio during the Cenozoic was in the early to mid-Eocene from 55 to 45 Ma. The pronounced shift from 17 to 22 per mil over a period of <10 My indicates that large changes in the external forcing mechanisms, such as tectonic uplift and weathering, volcanism, or oceanic vertical mixing and productivity (*22, 24*), influenced the fluxes and isotopic compositions of S input or burial, or both. Possible explanations for this increase include (i) a reduction of the river input of S to the ocean (by ~30% over 10 My) without changing the S output and sulfate/sulfide ratio, thus causing a decrease of ~20% in the seawater S concentration; (ii) a pronounced decrease in hydrothermal activity or volcanism; and (iii) a large increase in the rate of pyrite formation and burial relative to that of sulfates. Evidence for significant decreases in volcanic activity as volcanism in the North Atlantic and Caribbean decreased sharply at ~55 Ma (*23*) exists for this time interval. No direct evidence for increased input fluxes from the continents starting around 55 Ma exists, but the initial collision between India and Asia occurred then (*25*). Could the S curve be a manifestation of early uplift and weathering caused by the collision, as may be suggested by the cooling trend between 55 and 40 Ma (*26*) and supported by the $^{187}Os/^{186}Os$ shift toward more radiogenic values (*27*)? Intensified weathering and increased input of nutrients to the ocean would enhance marine biological productivity and sedimentation rates. These effects would promote increased pyrite formation and burial, which is limited by the availability of marine organic carbon (*22, 28*) and would lead to higher seawater $\delta^{34}S$ values. A combination of the second and third possibilities is the most likely explanation for this isotopic increase.

In the Oligocene to Pliocene, a 35-My period during which Earth experienced significant tectonic and climate changes, including the initiation and intensification of Ant-

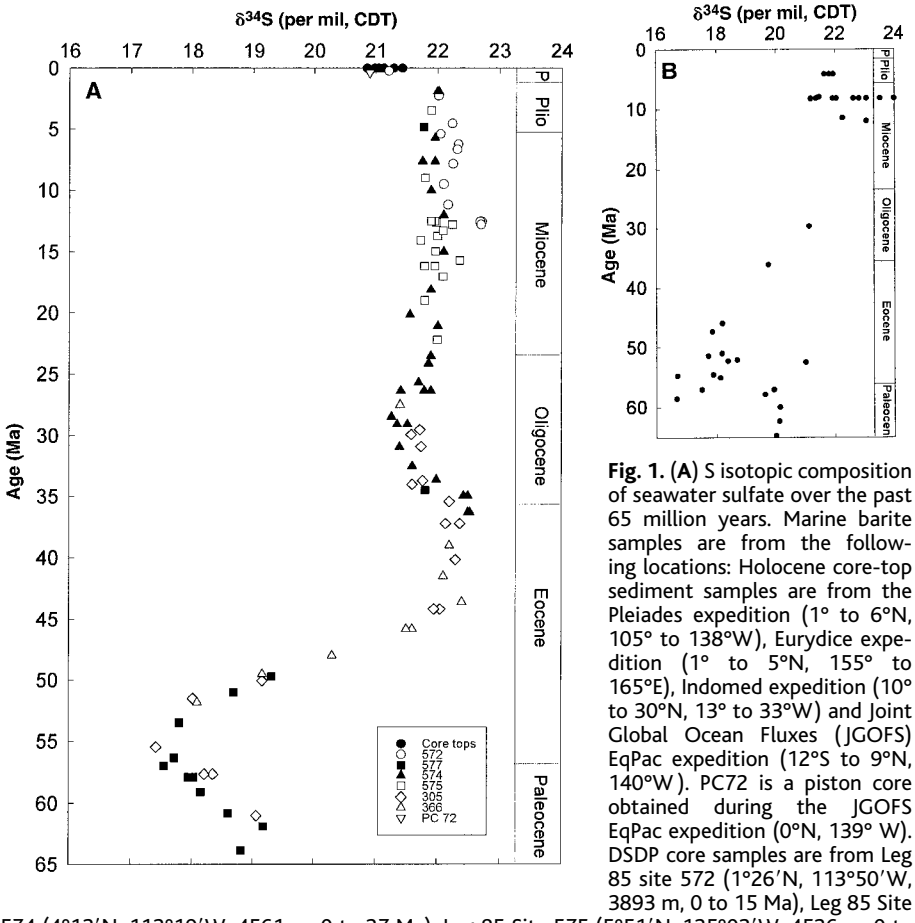

Fig. 1. (**A**) S isotopic composition of seawater sulfate over the past 65 million years. Marine barite samples are from the following locations: Holocene core-top sediment samples are from the Pleiades expedition (1° to 6°N, 105° to 138°W), Eurydice expedition (1° to 5°N, 155° to 165°E), Indomed expedition (10° to 30°N, 13° to 33°W) and Joint Global Ocean Fluxes (JGOFS) EqPac expedition (12°S to 9°N, 140°W). PC72 is a piston core obtained during the JGOFS EqPac expedition (0°N, 139° W). DSDP core samples are from Leg 85 site 572 (1°26′N, 113°50′W, 3893 m, 0 to 15 Ma), Leg 85 Site 574 (4°12′N, 113°19′W, 4561 m, 0 to 37 Ma), Leg 85 Site 575 (5°51′N, 135°02′W, 4536 m, 0 to 22 Ma), Leg 86 Site 577 (32°26′N, 157°43′W, 2675 m, 0 to 65 Ma), Leg 32 Site 305 (32°26′N, 157°50′E, 2675 m, 27 to 65 Ma), and Leg 41 Site 366 (3°26′N, 9°50′W, 2853 m, 25 to 65 Ma). (**B**) S isotope curve over the past 65 My, obtained from evaporites [data from (*6*)]. All the S isotopic ratios are reported in per mil relative to the Canyon Diablo Troilite standard and are plotted with respect to the chronology in (*41*). The sulfur isotope data are available on request from the corresponding author.

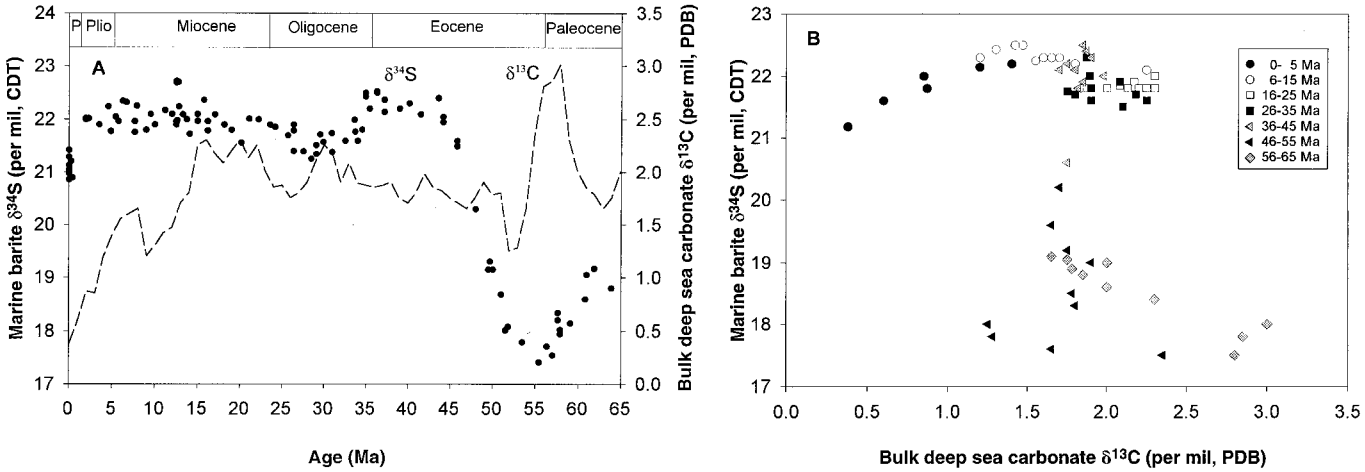

Fig. 2. (**A**) Cenozoic seawater sulfate S isotope record (this work) and bulk deep-sea sediment carbonate $\delta^{13}C$ record (*30*) averaged over 1-My increments with respect to the chronology in (*41*). (**B**) A plot of the S isotopic composition in marine barite versus the C isotopic composition of marine carbonate during the Cenozoic. The data are grouped according to age.

arctic glaciation, closure of the Mediterranean basin and of the Central American Isthmus, and intensified uplift and denudation in the Himalayas (*25, 29, 30*), the oceanic sulfate $\delta^{34}S$ value varied by <2 per mil (Fig. 1). The only pronounced feature of the isotopic record in the last 35 My is the small minimum in the Oligocene (at ~30 Ma), also observed in the evaporite record (*6*), which most likely represents a decrease in pyrite burial rates. The pronounced $\delta^{34}S$ decrease, of ~0.8 per mil in the last ~2 My, may also indicate a decrease in the pyrite burial rate, possibly because of a higher degree of ventilation and oxidation of deep water as it forms at cold high latitudes. This and the Oligocene shifts are also manifested in the C isotopic record (*30*) (Fig. 2A). An increase in the relative input of lighter S isotopes as a result of increased weathering, as indicated by the seawater Sr isotopic curve, could also cause this shift.

S and C isotope coupling and implications for atmospheric O_2. Burial and oxidation of organic carbon and sulfide S are considered the dominant controls on the mass of atmospheric oxygen (*1, 2, 9, 22, 24, 28, 31*). Geological evidence suggests that the mass of atmospheric oxygen has not decreased or increased by more than a factor of ~2 of the present amount (~38×10^{18} moles) since the Cambrian (*32*). Accordingly, major shifts in the redox state of S in the environment must have been balanced by complementary redox-state shifts of C, resulting in the expectation of a negative correlation between $\delta^{34}S_{sulfate}$ and $\delta^{13}C_{carbonate}$ at any given time. The $\delta^{34}S_{sulfate}$ and $\delta^{13}C_{carbonate}$ records provide estimates for the relative partitioning of C and S between their respective oxidized and reduced reservoirs through time. These records have been extensively used in models to assess the history of atmospheric P_{O_2} as well as the histories of C and S burial and weathering fluxes. When these isotopic data are averaged over time periods of ≥50 My, for the Phanerozoic, a negative correlation between $\delta^{34}S_{sulfate}$ and $\delta^{13}C_{carbonate}$ is observed (*33*). A comparison between the detailed $\delta^{13}C$ curve of marine carbonates, averaged over 1-My intervals (*30*), and the 1-My-resolution S isotope curve presented here (Fig. 2A) reveals no such correlation nor other significant correlations (Fig. 2B), suggesting that the changes in organic C and pyrite S burial rates do not balance each other over short time scales of a few million years or less. Using these two isotopic data sets in a model such as described by Kump and Garrels (*24*), in which the atmospheric oxygen level is driven solely by sulfide S and organic C burials, yields fluctuations in atmospheric oxygen concentration during the Cenozoic of >20%. Either such changes in atmospheric oxygen concentration have occurred or the stability of atmospheric oxygen concentration has been maintained, but not solely by the coupling between the C and S cycles, especially on time scales of 1 My to several million years. A deeper understanding of all the processes that influence the oxygen budget is needed before atmospheric oxygen fluctuations can be modeled reliably using the S and C isotope data of seawater sulfate and carbonate. These processes include the recently suggested involvement of the phosphorus cycle (*34*), hydrothermal and volcanic activities (*9, 35*), and iron oxidation (*36*). More elaborate models with negative feedback mechanisms that provide limits on atmospheric P_{O_2} excursions are needed to produce a realistic history of atmospheric O_2.

The observation that the $\delta^{34}S_{sulfate}$ and $\delta^{13}C_{carbonate}$ records do not correlate on time scales of 1 My to several million years (Fig. 2) is a consequence of the great difference in the residence times and oceanic reservoir sizes of C (10^5 years and 2×10^{18} moles, respectively) and S (2×10^7 years and 39×10^{18} moles, respectively) (*5, 22, 37*). Thus, the time required for the oceanic C and S concentrations and isotope ratios to reach a new steady state in response to input or output flux perturbations differs substantially; consequently, the oceanic C and S systems may be decoupled by millions of years (*22, 38*). Another factor that would preclude the suggested inverse relation between marine $\delta^{34}S_{sulfate}$ and $\delta^{13}C_{carbonate}$ is the observation that in normal marine settings, the amount of metabolizable organic matter is the most important limiting factor for bacterial sulfate reduction processes (*39*). This dependence results in a positive correlation between the burial rates of organic carbon and pyrite sulfur, as documented in both modern and ancient marine environments (*39, 40*). Because organic C and pyritic S are enriched in the lighter isotopes, their increased burial rates would shift the oceanic $\delta^{34}S_{sulfate}$ and $\delta^{13}C_{carbonate}$ to higher values and would lead to a positive correlation between these two parameters. The increased atmospheric O_2 concentration resulting from increased organic carbon burial will be amplified by the S cycle (*9, 22*).

References and Notes

1. W. T. Holser, M. Schidlowski, F. T. Mackenzie, J. B. Maynard, in *Chemical Cycles in the Evolution of Earth,* C. B. Gregor, R. M. Garrels, F. T. Mackenzie, J. B. Maynard, Eds. (Wiley, New York, 1988), pp. 105–173.
2. W. T. Holser, J. B. Maynard, K. M. Cruikshank, in *Evolution of the Global Biogeochemical Sulfur Cycle,* P. Brimbelcombe and A. Yu. Lein, Eds. (Wiley, New York, 1989), pp. 21–56; R. A. Berner and D. E. Canfield, *Am. J. Sci.* **289**, 333 (1989); L. R. Kump, *ibid.,* p. 390; A. D. Lasaga, *ibid.,* p. 411.
3. H. Strauss, *Palaeogeogr. Palaeoclimatol. Palaeoecol.* **132**, 97 (1997).
4. H. G. Thode and J. Monster, *Am. Assoc. Pet. Geol. Mem.* **4**, 367 (1965).
5. W. T. Holser and I. R. Kaplan, *Chem. Geol.* **1**, 93 (1966).
6. G. E. Claypool, W. T. Holser, I. R. Kaplan, H. Sakai, I. Zak, *ibid.* **28**, 199 (1980).
7. L. A. Chambers and P. A. Trudinger, *Geomicrobiol. J.* **1**, 249 (1978); R. E. Sweeney and I. R. Kaplan, *Mar. Chem.* **9**, 165 (1979).
8. A. Yu. Lein, in *The Global Biogeochemical Sulfur Cycle*, M. V. Ivanov and J. R. Freney, Eds. (Wiley, Chichester, UK, 1983), pp. 95–129; A. Yu. Lein and M. V. Ivanov, in *Evolution of the Global Biogeochemical Sulfur Cycle,* P. Brimbelcombe and A. Yu. Lein, Eds. (Wiley, New York, 1989), pp. 65–73.
9. J. C. G. Walker, *Mar. Geol.* **70**, 159 (1986).
10. H. Strauss, *Precambrian Res.* **63**, 225 (1993).
11. A. Longinelli, *Palaeogeogr. Palaeoclimatol. Palaeoecol.* **29**, 95 (1980); L. Hardie, *Am. J. Sci.* **284**, 193 (1984); H. Nielsen, in *Evolution of the Global Biogeochemical Sulfur Cycle,* P. Brimbelcombe and A. Yu. Lein, Eds. (Wiley, New York, 1989), pp. 57–64; M. Raab and B. Spiro, *Chem. Geol.* **86**, 323 (1991).
12. J. W. Burdett, M. A. Arthur, M. Richardson, *Earth Planet. Sci. Lett.* **94**, 189 (1989).
13. R. B. Lorens and M. L. Bender, *Geochim. Cosmochim. Acta* **44**, 1265 (1980); N. E. Pingitore Jr., G. Meitzner, K. M. Love, *ibid.* **59**, 2477 (1995).
14. P. A. Baker, J. M. Gieskes, H. Elderfield, *J. Sediment. Petrol.* **52**, 71 (1982); M. L. Delaney, *Earth Planet. Sci. Lett.* **95**, 23 (1989); W. T. Holser, *Paleoceanography* **3**, 173 (1988).
15. T. Church, in *Marine Barite in Marine Minerals, Short Course Notes*, vol. 6, R. G. Burns, Ed. (Mineralogical Society of America, Washington, DC, 1979), pp. 175–209.
16. A. Paytan, M. Kastner, E. E. Martin, J. D. Macdougall, T. Herbert, *Nature* **366**, 445 (1993).
17. A. Paytan, thesis, University of California, San Diego (1995).
18. Barite was separated from sediments by sequential leaching. The marine sediments were first leached with 6 N HCl in a glove bag under a N_2 atmosphere to remove the carbonate and sulfides. After ~12 hours, the acid was washed by centrifugation and the samples were treated as described (*16, 17*).
19. X. Gao and M. H. Thiemens, *Geochim. Cosmochim. Acta* **57**, 3159 (1993).
20. Barite was reacted with a reducing solution (HCl-HI-H_3PO_2) that converts barite sulfur to H_2S at 100% efficiency. The evolved H_2S was continually swept with a high-purity nitrogen carrier gas through a 0.2 M cadmium acetate trap. Hydrogen sulfide reacts with cadmium acetate to form CdS; its S was subsequently converted to Ag_2S by overnight reaction with 0.1 M $AgNO_3$. After yield determination, Ag_2S sulfur was converted to SF_6 by reaction with BrF_5 in a nickel reaction manifold. The reaction was carried out at 800°C for 12 hours with a 150-fold excess of BrF_5. After this reaction, the SF_6 was cryogenically purified by passage through a series of three traps at –118°C. A final purification was accomplished by means of a HP 5890A gas chromatograph (12 foot Porpak Q column). This final purification ensured the highest SF_6 purity. Three sulfur isotope ratios were measured ($^{36}S/^{34}S$, $^{34}S/^{32}S$, $^{33}S/^{32}S$) using a Finnigan MAT 252 triple-collector isotope ratio mass spectrometer. On the basis of >1000 sample and standard analyses, the precision and accuracy for $\delta^{34}S$ is 0.20 per mil. This includes the entire chemical extraction procedure, conversion to silver sulfide, purification, and mass spectrometry.
21. C. E. Rees, W. J. Jenkins, J. Monster, *Geochim. Cosmochim. Acta* **42**, 377 (1978).
22. S. T. Petsch and R. A. Berner, *Am. J. Sci.* **298**, 246 (1998).
23. D. K. Rea, J. C. Zachos, R. M. Owen, P. D. Gingerich, *Palaeogeogr. Palaeoclimatol. Palaeoecol.* **79**, 117 (1990); J. P. Kennett and J. P. Scott, *Nature* **353**, 225 (1991); P. L. Koch, J. C. Zachos, P. D. Gingerich, *ibid.* **358**, 319 (1992); E. Thomas and N. J. Shackleton, in *Correlation of the Early Paleoogene in Northwest Europe*, R. W. Knox, R. M. Corfield, R. E. Dunay, Eds.

(Geological Society Special Publication 101, 1996), pp. 401–441; T. J. Bralower *et al*., *Geology* **25**, 963 (1997).
24. L. R. Kump and R. M. Garrels, *Am. J. Sci.* **286**, 337 (1986).
25. M. E. Raymo, W. F. Ruddiman, P. N. Froelich, *Geology* **16**, 649 (1988); R. A. Beck *et al*., *Nature* **373**, 55 (1995); R. A. Beck, D. W. Burbank, W. J. Sercombe, T. L. Olson, A. M. Khan, *Geology* **23**, 387 (1995).
26. K. G. Miller, R. G. Fairbanks, G. S. Mountain, *Paleoceanography* **2**, 1 (1987); W. F. Ruddiman, *Nature* **394**, 723 (1998).
27. B. Peucker-Ehrenbrink, G. Ravizza, A. W. Hofmann, *Earth Planet. Sci. Lett.* **130**, 155 (1995).
28. R. A. Berner, *Palaeogeogr. Palaeoclimatol. Palaeoecol.* **75**, 97 (1989).
29. W. H. Berger, V. S. Smetacek, G. Wefer, Eds., *Ocean Productivity and Paleoproductivity—An Overview* (Wiley, New York, 1989); M. L. Delaney and E. A. Boyle, *Paleoceanography* **3**, 137 (1988); G. H. Rau, in *Carbon Cycling in the Glacial Ocean Constrains on the Oceanic Role in Global Change: Quantitative Approaches in Paleoceanography,* R. Zahn, T. F. Pedersen, M. A. Kaminski, L. Labeyrie, Eds. (Springer-Verlag, Berlin, 1994), pp. 307–321; J. C. Zachos, L. D. Scott, K. C. Lohmann, *Paleoceanography* **9**, 353 (1994).
30. W. J. Shackleton, in *Marine Petroleum Source Rocks,* J. Brooks and A. J. Fleet, Eds. (Geological Society, London, 1987), pp. 423–434.
31. This is represented by the following two chemical equations

$$CO_2 + H_2O \underset{\text{weathering}}{\overset{\text{burial}}{\rightleftharpoons}} CH_2O + O_2 \quad (1)$$

$$2Fe_2O_3 + 16Ca^{2+} + 16HCO_3^- + 8SO_4^{2-} \underset{\text{weathering}}{\overset{\text{burial}}{\rightleftharpoons}} 4FeS_2 + 16CaCO_3 + 8H_2O + 15O_2 \quad (2)$$

[H. D. Holland, *The Chemical Evolution of the Atmospheres and Oceans* (Princeton Univ. Press, Princeton, NJ, 1984); H. D. Holland, *Geochim. Cosmochim. Acta* **37**, 2605 (1973); R. M. Garrels and E. A. Perry Jr., in *The Sea, 5, Marine Chemistry,* E. D. Goldberg, Ed. (Wiley, New York, 1974); R. M. Garrels, A. Lerman, F. T. Mackenzie, *Am. Sci.* **63**, 306 (1976); M. Schidlowski, C. E. Junge, H. Pietrek, *J. Geophys. Res.* **82**, 2557 (1977); R. M. Garrels and A. Lerman, *Am. J. Sci.* **284**, 989 (1984); R. A. Berner, *ibid.* **287**, 177 (1987); F. T. Mackenzie, L. M. Ver, C. Sabine, M. Lane, A. Lerman, in *Interactions of C, N, P, and S Biogeochemical Cycles and Global Change* (NATO ASI Series, 1993), vol. 14, pp. 1–62].
32. L. V. Berkner and L. C. Marshall, *J. Atmos. Sci.* **22**, 225 (1965); A. Watson, J. E. Lovelock, L. Margulis, *Biosystems* **10**, 293 (1978); T. P. Jones and W. G. Chaloner, *Palaeogeogr. Palaeoclimatol. Palaeoecol.* **77**, 39 (1991); J. M. Robinson, *ibid.,* p. 51.
33. J. Veizer, W. T. Holser, C. K. Wilgus, *Geochim. Cosmochim. Acta* **44**, 579 (1980); T. B. Lindh, thesis, University of Miami (1983).
34. P. Van Cappellen and E. D. Ingall, *Science* **271**, 493 (1996); A. S. Colman, H. D. Holland, F. T. Mackenzie, *ibid.* **275**, 406 (1997).
35. S. J. Carpenter and K. C. Lohmann, *Geochim. Cosmochim. Acta* **61**, 4831 (1997).
36. M. Schidlowski and C. E. Junge, *ibid.* **45**, 589 (1981).
37. J. Hoefs, in *Hand Book of Geochemistry,* K. H. Wedepohl, Ed. (Springer-Verlag, Berlin, 1967), vol. I-6.
38. S. T. Petsch, *Geochim. Cosmochim. Acta,* in press.
39. R. A. Berner, *ibid.* **48**, 605 (1984).
40. _____ and R. Raiswell, *ibid.* **47**, 855 (1983); R. Raiswell and R. A. Berner, *ibid.* **50**, 1967 (1986).
41. S. C. Cande and D. V. Kent, *J. Geophys. Res.* **100**, 6093 (1995).
42. Supported by NSF grant EAR-9628479. Cores were provided by the Ocean Drilling Program. We thank T. Jackson for help with sample analysis.

27 July 1998; accepted 25 September 1998

High-Resolution Protein Design with Backbone Freedom

Pehr B. Harbury,* Joseph J. Plecs, Bruce Tidor, Tom Alber, Peter S. Kim†

Recent advances in computational techniques have allowed the design of precise side-chain packing in proteins with predetermined, naturally occurring backbone structures. Because these methods do not model protein main-chain flexibility, they lack the breadth to explore novel backbone conformations. Here the de novo design of a family of α-helical bundle proteins with a right-handed superhelical twist is described. In the design, the overall protein fold was specified by hydrophobic-polar residue patterning, whereas the bundle oligomerization state, detailed main-chain conformation, and interior side-chain rotamers were engineered by computational enumerations of packing in alternate backbone structures. Main-chain flexibility was incorporated through an algebraic parameterization of the backbone. The designed peptides form α-helical dimers, trimers, and tetramers in accord with the design goals. The crystal structure of the tetramer matches the designed structure in atomic detail.

Proteins exhibit precise geometric packing of atoms in their interiors. Nevertheless, empirical protein design methods have achieved a measure of generality and simplicity by ignoring detailed interactions between amino acid residues. These design approaches rely instead on imitation of statistical sequence patterns in naturally occurring proteins, such as hydrophobic-polar residue patterns, amino acid secondary structure propensities, and characteristic local interaction motifs (*1*). Perhaps as a direct consequence, many designed proteins exhibit fluctuating or "molten" interiors (*2*), and some assume unintended tertiary conformations (*3*).

Packing in proteins has been studied computationally by holding the protein main chain in the wild-type conformation (the "fixed-backbone" approximation) and asking which sets of amino acid side chains can efficiently fill the interior space (*4*). This technique has been used successfully to repack wild-type side chains into predetermined backbone structures (*5*) and has more recently been extended to the design of amino acid sequences. Fixed-backbone design based on naturally occurring backbone templates has produced proteins that fold to the target structures with high thermal stabilities (*6*).

However, fixed-backbone methods are unable to model protein main-chain flexibility. Thus, main-chain adjustments known to occur in response to core mutations in proteins (*7*) are not allowed. Moreover, the fixed-backbone approach has a severe limitation when applied to backbone structures for which a naturally occurring example does not exist. Although naturally occurring backbone coordinates represent the ground-state conformation for at least one sequence (the naturally occurring sequence), this assumption is not necessarily valid for arbitrary backbone coordinates. When the backbone structure is designed de novo, a complete set of plausible backbone conformations must be sampled to identify structures that lie at a free-energy minimum in the sequence and conformational spaces.

These limitations may be overcome by treating the backbone as a parametric family of structures rather than as a static entity (*8*). A small but well-defined subset of main-chain conformations can then be exhaustively sampled in a finite time. For example, coupled searches of side-chain packing and main-chain conformation under a parametric coiled-coil backbone model have been used to reproduce detailed, crystallographically observed conformations for coiled-coil proteins (*8*).

A true test of the utility of parametric-backbone models in protein design would be to engineer a protein fold for which no structural example is known. We report here the computational design of a family of dimeric, trimeric, and tetrameric α-helical bundles

P. B. Harbury is at the Whitehead Institute for Biomedical Research, Howard Hughes Medical Institute and Department of Biology, Massachusetts Institute of Technology, Nine Cambridge Center, Cambridge, MA 02142, USA, and Department of Biological Chemistry and Molecular Pharmacology, Harvard Medical School, Boston, MA 02115, USA. J. J. Plecs is in the Department of Molecular and Cell Biology and Department of Physics, University of California at Berkeley, Berkeley, CA 94720, USA. B. Tidor is in the Department of Chemistry, Massachusetts Institute of Technology, Cambridge, MA 02139, USA. T. Alber is in the Department of Molecular and Cell Biology, University of California at Berkeley, Berkeley, CA 94720, USA. P. S. Kim is at the Whitehead Institute for Biomedical Research, Howard Hughes Medical Institute and Department of Biology, Massachusetts Institute of Technology, Nine Cambridge Center, Cambridge, MA 02142, USA.

*Present address: Department of Biochemistry, Stanford University, Stanford, CA 94305, USA.
†To whom correspondence should be addressed. E-mail: dvorak@wi.mit.edu